are needed to identify the mechanisms involved in the hypotensive effects of vagal nerve stimulation observed in SHR.

Limitation

Several limitations to the present study need to be addressed. First, to avoid the degradation of ACh, an acetylcholinesterase inhibitor eserine was added to the perfusate. Although myocardial interstitial ACh levels measured by cardiac microdialysis have been shown to reflect changes in the ACh kinetics induced by pharmacological or pathological interventions (Kawada *et al.* 2000, 2001), the results have to be interpreted carefully. Second, because of the different perfusion rates, the ACh levels obtained in Protocols 1 and 2 cannot be compared directly. For instance, the lower baseline ACh levels in Protocol 2 compared to Protocol 1 are not necessarily the results of vagotomy. Third, we measured myocardial interstitial ACh levels in the left ventricle and not in the right atrium near the sinoatrial node. Although we assumed that changes in ACh level account for the alterations in HR induced by the vagal nerve, changes in ACh level in the ventricle may not be proportional to changes in the sinoatrial node. Finally, the experiments were carried out on rats at an age when hypertension in SHR is well established. Further studies are required to determine whether the abnormality of central vagal activation in SHR occurs at an earlier age before hypertension is developing.

Conclusion

Alpha$_2$-adrenergic stimulation induced the central vagal activation in WKY, but this mechanism was impaired in SHR. In addition to abnormal sympathetic control, vagal control by the central nervous system may be impaired in SHR. On the other hand, peripheral vagal control of ACh release and HR response may be preserved in SHR.

Conflict of interest

The authors declared no conflict of interest.

This study was supported by Health and Labour Sciences Research Grants (H19-nano-Ippan-009, H20-katsudo-Shitei-007 and H21-nano-Ippan-005) from the Ministry of Health, Labour and Welfare of Japan; and by the Grant-in-Aid for Scientific Research (23592319, 23·01705) promoted by the Ministry of Education, Culture, Sports, Science and Technology of Japan; and by the Industrial Technology Research Grant Program from the New Energy and Industrial Technology Development Organization (NEDO) of Japan.

References

Akiyama, T., Yamazaki, T. & Ninomiya, I. 1994. In vivo detection of endogenous acetylcholine release in cat ventricles. *Am J Physiol* **266**, H854–H860.

Akiyama, T., Yamazaki, T., Mori, H. & Sunagawa, K. 2004. Simultaneous monitoring of acetylcholine and catecholamine release in the in vivo rat adrenal medulla. *Neurochem Int* **44**, 497–503.

Boychuk, C.R., Bateman, R.J., Philbin, K.E. & Mendelowitz, D. 2011. α_1-adrenergic receptors facilitate inhibitory neurotransmission to cardiac vagal neurons in the nucleus ambiguus. *Neuroscience* **193**, 154–161.

Corbett, E.K., Mary, D.A., McWilliam, P.N. & Batten, T.F. 2007. Age-related loss of cardiac vagal preganglionic neurones in spontaneously hypertensive rats. *Exp Physiol* **92**, 1005–1013.

Ferrari, A.U., Daffonchio, A., Franzelli, C. & Mancia, G. 1992. Cardiac parasympathetic hyperresponsiveness in spontaneously hypertensive rats. *Hypertension* **19**, 653–657.

Glantz, S.A. 2002. *Primer of Biostatistics*, 5th edn, McGraw-Hill, New York.

Heaton, D.A., Li, D., Almond, S.C., Dawson, T.A., Wang, L., Channon, K.M. & Paterson, D.J. 2007. Gene transfer of neuronal nitric oxide synthase into intracardiac ganglia reverses vagal impairment in hypertensive rats. *Hypertension* **49**, 380–388.

Jablonskis, L.T. & Howe, P.R. 1994. Lack of influence of circulating adrenaline on blood pressure in normotensive and hypertensive rats. *Blood Press* **3**, 112–119.

Kambayashi, M., Miura, T., Oh, B.H., Rockman, H.A., Murata, K. & Ross, J. Jr 1992. Enhancement of the force-frequency effect on myocardial contractility by adrenergic stimulation in conscious dogs. *Circulation* **86**, 572–580.

Kawada, T., Yamazaki, T., Akiyama, T., Sato, T., Shishido, T., Inagaki, M., Takaki, H., Sugimachi, M. & Sunagawa, K. 2000. Differential acetylcholine release mechanisms in the ischemic and non-ischemic myocardium. *J Mol Cell Cardiol* **32**, 405–414.

Kawada, T., Yamazaki, T., Akiyama, T., Shishido, T., Inagaki, M., Uemura, K., Miyamoto, T., Sugimachi, M., Takaki, H. & Sunagawa, K. 2001. In vivo assessment of acetylcholine-releasing function at cardiac vagal nerve terminals. *Am J Physiol Heart Circ Physiol* **281**, H139–H145.

Kawada, T., Akiyama, T., Shimizu, S., Kamiya, A., Uemura, K., Li, M., Shirai, M. & Sugimachi, M. 2009. Detection of endogenous acetylcholine release during brief ischemia in the rabbit ventricle: a possible trigger for ischemic preconditioning. *Life Sci* **85**, 597–601.

Kawada, T., Akiyama, T., Shimizu, S., Kamiya, A., Uemura, K., Sata, Y., Shirai, M. & Sugimachi, M. 2010. Large conductance Ca^{2+}-activated K^+ channels inhibit vagal acetylcholine release at the rabbit sinoatrial node. *Auton Neurosci* **156**, 149–151.

Kawada, T., Shimizu, S., Li, M., Kamiya, A., Uemura, K., Sata, Y., Yamamoto, H. & Sugimachi, M. 2011. Contrasting effects of moderate vagal stimulation on heart rate and

carotid sinus baroreflex-mediated sympathetic arterial pressure regulation in rats. *Life Sci* **89**, 498–503.

Kuusela, E., Raekallio, M., Anttila, M., Falck, I., Mölsä, S. & Vainio, O. 2000. Clinical effects and pharmacokinetics of medetomidine and its enantiomers in dogs. *J Vet Pharmacol Ther* **23**, 15–20.

Mancia, G., Grassi, G., Giannattasio, C. & Seravalle, G. 1999. Sympathetic activation in the pathogenesis of hypertension and progression of organ damage. *Hypertension* **34**, 724–728.

Masuda, Y. 2000. Role of the parasympathetic nervous system and interaction with the sympathetic nervous system in the early phase of hypertension. *J Cardiovasc Pharmacol* **36**(Suppl 2), S61–S64.

Matsuura, W., Sugimachi, M., Kawada, T., Sato, T., Shishido, T., Miyano, H., Nakahara, T., Ikeda, Y., Alexander, J. Jr & Sunagawa, K. 1997. Vagal stimulation decreases left ventricular contractility mainly through negative chronotropic effect. *Am J Physiol* **273**, H534–H539.

McDonough, P.M., Wetzel, G.T. & Brown, J.H. 1986. Further characterization of the presynaptic *alpha*-1 receptor modulating [^{3}H]ACh release from rat atria. *J Pharmacol Exp Ther* **238**, 612–617.

Minami, N. & Head, G.A. 2000. Cardiac vagal responsiveness during development in spontaneously hypertensive rats. *Auton Neurosci* **82**, 115–122.

Mitchell, J.H., Wallace, A.G. & Skinner, N.S. Jr 1963. Intrinsic effects of heart rate on left ventricular performance. *Am J Physiol* **205**, 41–48.

Nakayama, Y., Miyano, H., Shishido, T., Inagaki, M., Kawada, T., Sugimachi, M. & Sunagawa, K. 2001. Heart rate-independent vagal effect on end-systolic elastance of the canine left ventricle under various levels of sympathetic tone. *Circulation* **104**, 2277–2279.

Nalivaiko, E., Antunes, V.R. & Paton, J.F. 2010. Control of cardiac contractility in the rat working heart-brainstem preparation. *Exp Physiol* **95**, 107–119.

Nosaka, S. & Wang, S.C. 1972. Carotid sinus baroceptor functions in the spontaneously hypertensive rat. *Am J Physiol* **222**, 1079–1084.

Philbin, K.E., Bateman, R.J. & Mendelowitz, D. 2010. Clonidine, an α_2-receptor agonist, diminishes GABAergic neurotransmission to cardiac vagal neurons in the nucleus ambiguus. *Brain Res* **1347**, 65–70.

Robertson, H.A. & Leslie, R.A. 1985. Noradrenergic alpha$_2$ binding sites in vagal dorsal motor nucleus and nucleus tractus solitarius: autoradiographic localization. *Can J Physiol Pharmacol* **63**, 1190–1194.

Salgado, H.C., Barale, Á.R., Castania, J.A., Machado, B.H., Chapleau, M.W. & Fazan, R. Jr 2007. Baroreflex responses to electrical stimulation of aortic depressor nerve in conscious SHR. *Am J Physiol Heart Circ Physiol* **292**, H593–H600.

Shimizu, S., Akiyama, T., Kawada, T., Shishido, T., Yamazaki, T., Kamiya, A., Mizuno, M., Sano, S. & Sugimachi, M. 2009. In vivo direct monitoring of vagal acetylcholine release to the sinoatrial node. *Auton Neurosci* **148**, 44–49.

Shimizu, S., Akiyama, T., Kawada, T., Sata, Y., Mizuno, M., Kamiya, A., Shishido, T., Inagaki, M., Shirai, M., Sano, S. & Sugimachi, M. 2012. Medetomidine, an α_2-adrenergic agonist, activates cardiac vagal nerve through modulation of baroreflex control. *Circ J* **76**, 152–159.

Sinclair, M.D. 2003. A review of the physiological effects of α_2-agonists related to the clinical use of medetomidine in small animal practice. *Can Vet J* **44**, 885–897.

Snedecor, G.W. & Cochran, W.G. 1989. *Statistical Methods*. 8th edn, pp. 290–291. Iowa State, Iowa.

Tsunoda, M., Takezawa, K., Santa, T., Ina, Y., Nagashima, K., Ohmori, K., Kobayashi, S. & Imai, K. 2000. New approach for measurement of sympathetic nervous abnormality in conscious, spontaneously hypertensive rats. *Jpn J Pharmacol* **83**, 39–45.

34th Annual International Conference of the IEEE EMBS
San Diego, California USA, 28 August - 1 September, 2012

Consideration on Parameter Determination of a New Model Describing Dynamic Vagal Heart Rate Control in Rats

Toru Kawada, Kazunori Uemura, Shuji Shimizu, Atsunori Kamiya, Michael J Turner, Masaki Mizuno, Kenji Sunagawa, *Member, IEEE*, and Masaru Sugimachi, *Member, IEEE*

Abstract— **The dynamic characteristics of vagal heart rate control can be approximated by a first-order low-pass filter with pure dead time in rabbits. However, this model may not necessarily be the best approximation of the vagal transfer function of the heart rate control in rats, because a flatter portion exists in the gain plot above approximately 0.3 Hz. We developed a new model that includes a frequency-independent gain term to reproduce the flatter portion of the gain plot seen in the vagal transfer function in rats. The inclusion of the new term increased the coefficient of determination in an external validation of the linear regression relationship between measured and predicted heart rate responses to vagal stimulation, and made the slope of the regression line closer to unity. The parameters of mathematical transfer functions were determined in both the frequency and time domains. The frequency-domain fitting provided a set of parameters that was also able to reproduce the time-domain step response reasonably well. In contrast, the time-domain fitting provided a set of parameters that reproduced the frequency-domain transfer function only up to 0.2 Hz. Determination of proper model parameters was crucial for the development of a new model to describe the dynamic heart rate response to vagal stimulation in rats.**

I. Introduction

Dynamic heart rate control is important to adjust cardiac function to meet demands in daily activity. Both sympathetic and vagal systems are involved in the control of heart rate. Our previous study showed that dynamic characteristics of vagal heart rate control could be approximated by a first-order low-pass filter with pure dead time in rabbits [1]. However, a first-order low-pass filter with pure dead time is not necessarily the best approximation for the vagal transfer function of heart rate control in rats, because the transfer gain does not fall off smoothly above the corner frequency [2]. The gain plot exhibits a flatter portion in the frequency-domain around 0.3 Hz and above, which makes the transfer function deviate from a simple first-order low-pass filter with pure dead time. To describe the flatter portion in the gain plot, we propose a new model that includes a frequency-independent gain term in addition to the terms describing the low-pass nature of the dynamic heart rate control. The parameters of the proposed model were determined by the frequency-domain and time-domain methods.

Manuscript received March 12, 2012. This work was supported in part by Health and Labour Sciences Research Grants (H20-katsudo-Shitei-007, H21-nano-Ippan-005) from the Ministry of Health, Labour and Walfare of Japan, and a grant-in-aid for Scientific Research (23592319) from the Ministry of Education, Culture, Sports, Science and Technology of Japan.

T. Kawada, K. Uemura, S. Shimizu, A. Kamiya, M. J. Turner are with Department of Cardiovascular Dynamics, National Cerebral and Cardiovascular Center, Osaka 565-8565, Japan (corresponding author: T. Kawada, phone +81-6-6833-5012, fax: +81-6-6835-5403, e-mail: torukawa@ri.ncvc.go.jp).

M. Mizuno is with Department of Health Care Sciences, University of Texas Southwestern Medical Center, Dallas, TX, USA.

K. Sunagawa is with Department of Cardiovascular Medicine, Graduate School of Medical Sciences, Kyushu University, Fukuoka 812-8582, Japan.

II. Methods

A. Animal Preparation

The study was performed on 6 anesthetized Sprague-Dawley rats. Animals were cared for in strict accordance with the Guiding Principles for the Care and Use of Animals in the Field of Physiological Sciences, which has been approved by the Physiological Society of Japan. All experimental protocols were reviewed and approved by the Animal Subjects Committee at National Cerebral and Cardiovascular Center.

The rats were anesthetized with an intraperitoneal injection (2 ml/kg) of a mixture of urethane (250 mg/ml) and α-chloralose (40 mg/ml), and ventilated mechanically with oxygen-supplied room air. Supplemental anesthetic mixture was administered continuously. Arterial pressure was monitored through a catheter inserted into the right femoral artery. Heart rate was measured from body surface electrocardiogram using a cardiotachometer. In order to minimize systemic changes in sympathetic nerve activity, baroreceptor regions at bilateral carotid sinuses were isolated from the systemic circulation, and the intracarotid sinus pressure was maintained at 120 mmHg using a servo-controlled piston pump [3], [4], [5]. The aortic depressor nerves and vagi were sectioned bilaterally at the neck. A pair of stainless steel wire electrodes (Bioflex wire, AS633, Cooner Wire, CA, USA) was attached to the sectioned distal end of the right vagus for electrical stimulation.

To estimate dynamic characteristics of the vagal heart rate control, the right vagus was stimulated for 15 min according to a binary white noise signal. The command signal was assigned to either 0 or 20 Hz every 0.5 s. As a result, the input power spectrum was relatively constant up to 1 Hz.

B. Data Analysis

Experimental data were stored at 1000 Hz using a 16-bit analog-to-digital converter. To avoid the possibility that the initial transition from zero stimulation to the binary white noise stimulation biasing the transfer function estimation, the data were analyzed starting 2 min after the initiation of

978-1-4577-1787-1/12/$26.00 ©2012 IEEE

stimulation. Input-output data pairs were resampled at 10 Hz, and partitioned into 10 half-overlapping segments consisting of 1024 data points each. In each segment, the linear trend was subtracted and a Hanning window was applied. Frequency spectra of the input $[X(f)]$ and the output $[Y(f)]$ were obtained via the fast Fourier transform. The input power $[S_{XX}(f)]$, output power $[S_{YY}(f)]$, and the cross spectra between the input and output $[S_{YX}(f)]$ were calculated over the 10 segments. Finally, the transfer function from vagal stimulation to the heart rate response was calculated using the following equation [6]:

$$H(f) = \frac{S_{YX}(f)}{S_{XX}(f)}$$

To quantify the linear dependence of the heart rate response to the vagal stimulation, the magnitude squared coherence function was calculated using the following equation:

$$Coh(f) = \frac{|S_{YX}(f)|^2}{S_{XX}(f) S_{YY}(f)}$$

To help intuitive understanding of the system behavior, the system step response was calculated from a time integral of the system impulse response which was derived from the inverse Fourier transform of the transfer function. Hereafter in this paper, this step response is referred to as an "nonparametric" step response.

In the original model (Model A) we used a first-order low-pass filter with pure dead time as described below [1].

$$M_A(f) = \frac{K}{1 + \frac{f}{f_C} j} \exp(-2\pi f L j)$$

where K is the steady-state gain, f_C is the corner frequency (in Hz), and L is the pure dead time (in s). j represents the imaginary units. The step response corresponding to Model A is as follows.

$$\begin{cases} S_A(t) = 0 & (t < L) \\ S_A(t) = K\left[1 - \exp\left(-\frac{t-L}{\tau}\right)\right] & (L \le t) \end{cases}$$

$$\tau = \frac{1}{2\pi f_C}$$

Our newly proposed model (Model B) is a combination of the first-order low-pass filter and a frequency-independent gain term as follows.

$$M_B(f) = K\left(\frac{\frac{1-R}{1 + \frac{f}{f_C} j} + R}{}\right) \exp(-2\pi f L j)$$

where R $(0 \le R < 1)$ represents the fraction of the frequency-independent gain relative to the steady-state gain. Although other models could be possible, Model B is thought to be most convenient because it provides the steady-state gain by K as in Model A. When $R > 0$ Model B can be rewritten as:

$$M_B(f) = K\left(\frac{1 + \frac{f}{f_R} j}{1 + \frac{f}{f_C} j}\right) \exp(-2\pi f L j)$$

where $f_R = f_C / R$. Because R is defined as a value less than unity, f_R is greater than f_C. The step response corresponding to Model B is as follows.

$$\begin{cases} S_B(t) = 0 & (t < L) \\ S_B(t) = K\left[1 - (1-R)\exp\left(-\frac{t-L}{\tau}\right)\right] & (L \le t) \end{cases}$$

The model parameters were estimated in both the frequency domain and the time domain. In the time-domain fitting, the sum of squared errors between the model step response and the nonparametric step response was minimized using a nonlinear iterative least square fitting. In the frequency-domain fitting, the following error function was employed.

$$E = \sum_{k=1}^{N} \frac{[\log(H(f_k)) - \log(M(f_k))]^2}{k} = \sum_{k=1}^{N} \frac{1}{k}\left[\log\left(\frac{H(f_k)}{M(f_k)}\right)\right]^2$$

$$f_k = f_0 \times k$$

where f_0 is the fundamental frequency of the Fourier transform, k is an index of the frequency, and f_k is the k-th frequency. N represents the frequency index up to which the error was considered. In the present study, N was set at 120, which corresponded to 1.17 Hz. $H(f)$ and $M(f)$, which are both complex values, represent the experimental and model transfer functions, respectively. The error function took the logarithmic representation of the system dynamic characteristics on the Bode plot into account. In this context, there was no difference whether the natural or common logarithm were used, as the task of fitting was to find a set of parameters to minimize the error function.

After the model parameters were estimated, the dynamic heart rate response to vagal stimulation was predicted from the convolution of the command signal with the impulse response derived from the model transfer function. The regression analysis for the measured versus the predicted heart rate response was performed using a data set that was obtained externally to the segments used for the estimation of the transfer function (i.e., external validation). The output signal of 2048 points was predicted.

III. Results and Discussion

Figure 1 illustrates a typical example of the transfer function from vagal stimulation to the heart rate response obtained in one animal (solid lines). In the gain plot, the transfer gain decreased as the frequency increased above 0.02 Hz, suggesting low-pass characteristics of the heart rate response to vagal stimulation. The transfer gain, however, did not fall off smoothly beyond 0.3 Hz, creating a flatter portion in the higher frequency range. In the phase plot, the phase was close to $-\pi$ radians at the lowest frequency, and delayed with increasing frequency. These phase characteristics suggest that the heart rate response to vagal stimulation should be negative

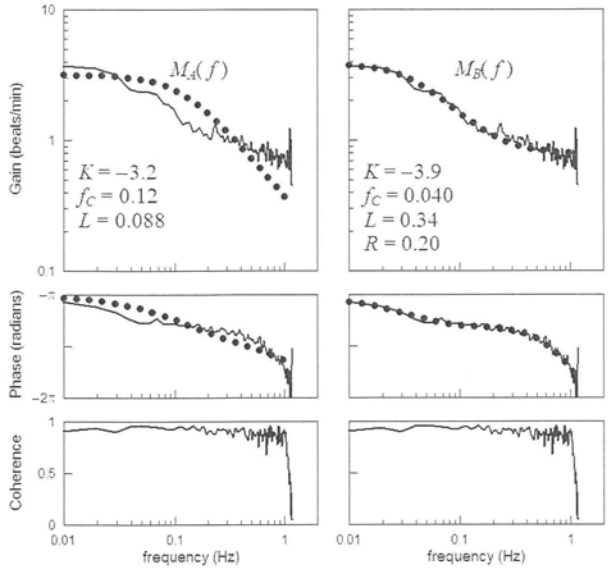

Figure 1. Transfer function from vagal stimulation to the heart rate response (solid lines) and model tranfer functions (circled lines).

at steady state. The coherence was high up to 1 Hz, suggesting that the heart rate response can mostly be described by linear dynamics in the present experimental settings. Therefore, the flatter portion observed in the gain plot is not likely the result of a reduction in the accuracy of the transfer function estimation in the higher frequency range.

The circles in the left panels of Figure 1 represent the transfer function of Model A with its parameters determined by the frequency-domain fitting. There was a significant deviation between Model A and experimental transfer functions such that the steady-state gain was estimated to be lower in Model A compared with the experimental transfer function. The corner frequency was estimated to be higher in Model A than in the experimental transfer function. Therefore, frequency-domain parameter determination does not work well when a given model does not have the degree of freedom

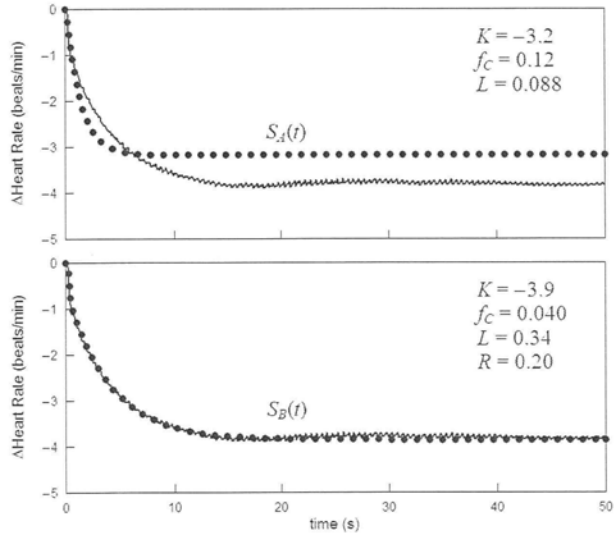

Figure 2. Step response of the heart rate response to vagal stimulation (solid lines) and model step responses based on the frequency-domain parameter determination (circles).

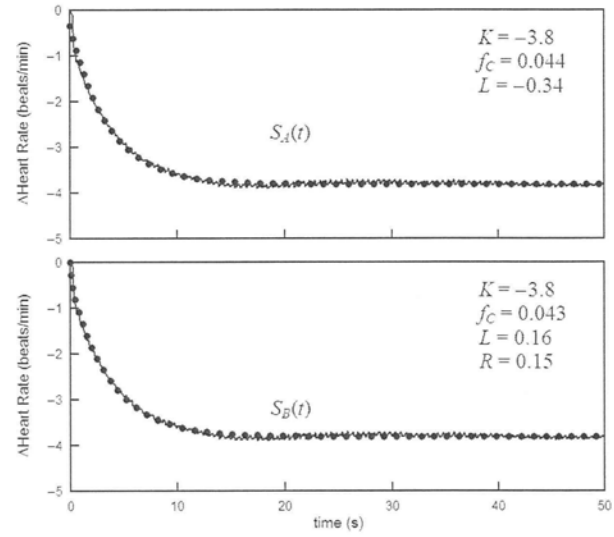

Figure 3. Step response of the heart rate response to vagal stimulation (solid lines) and model step responses based on the time-domain parameter determination (circled lines).

to reproduce an experimental transfer function.

The circles in the right panels of Figure 1 indicate the transfer function of Model B with its parameters determined by the frequency-domain fitting. The model transfer function reproduced the characteristics of the experimental transfer function reasonably well in the frequency range from 0.01 to 1 Hz.

Figure 2 depicts the step responses corresponding to the transfer functions shown in Figure 1. In the top panel, the step response of Model A underestimated the steady-state response relative to that of the nonparametric step response. The time constant was estimated to be shorter, which is equivalent to the higher corner frequency in the frequency domain. In the bottom panel, the step response of Model B reproduced the nonparametric step response well.

While Model A did not reproduce the experimental step response well when parameters were determined in the frequency domain, both models A and B were able to mimic the nonparametric step response when parameters were determined in the time domain (Figure 3). However, the lag time was estimated to be negative in Model A, which is physically unrealizable.

Figure 4 illustrates the transfer function from vagal stimulation to the heart rate response (solid lines) and the model transfer functions (circles) with their parameters determined in the time domain to minimize the error between the model and nonparametric step responses. While both models A and B reproduced the experimental transfer function up to 0.2 Hz, the model transfer functions deviated from the experimental transfer function in the frequency range above 0.2 Hz. Therefore, even though the model step response appeared to mimic the nonparametric step response, there can be a significant deviation in the higher frequency range when examined in the frequency domain. In the present case, because the fraction of the frequency-independent gain relative to the steady-state gain was approximately 0.2, the

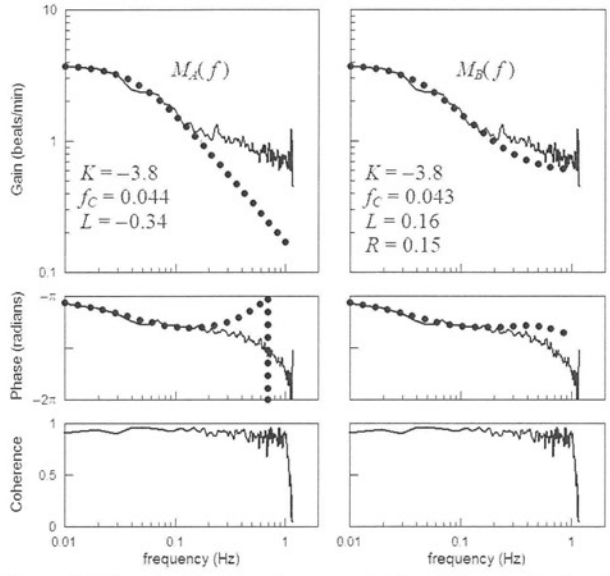

Figure 4. Transfer function from vagal stimulation to the heart rate response (solid lines) and model tranfer functions based on the time-domain parameter determination (circles).

majority of the step response could be described by the parameters relating to the first-order low-pass filter.

Figure 5 illustrates the actually measured dynamic heart rate response to vagal stimulation versus the heart rate responses predicted by Model A (top panel) and Model B (bottom panel). Close inspection of the figure indicates that Model A was not able to reproduce sharp rises in the heart rate response (marked with asterisks) in contrast with Model B. The scatter plots of the measured versus the predicted heart rate are shown in the right panels of Figure 5. The coefficient of determination was higher for the prediction when using Model B compared with Model A.

The regression analysis on data obtained from 6 rats shows that the slope of the regression line was 0.81±0.05 for the heart rate prediction by Model A, and was 0.94±0.03 for the heart rate prediction by Model B. In all six animals, the coefficient of determination was higher in the prediction by Model B (ranged from 0.71 to 0.91) than in the prediction by Model A (ranged 0.56 to 0.90). While the increment of the number of model parameters itself should increase the coefficient of determination, because the regression analysis was performed on a data set that was not used for the estimation of the transfer function (i.e., external validation), it may be fair to say that Model B provided a better prediction of the heart rate response compared with Model A.

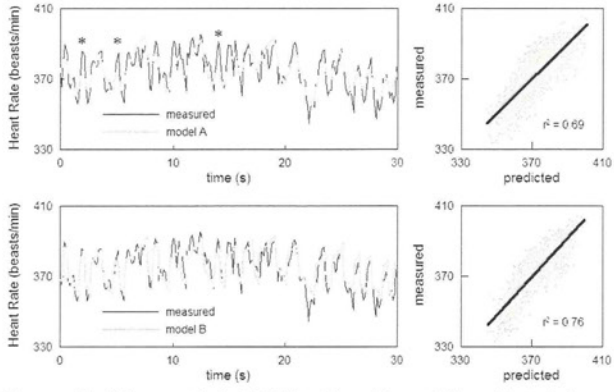

Figure 5. Measured (solid lines) and model-predicted (gray lines) of the heart rate response to vagal stimulation. The top panels are the results ofmodel A and the bottom panels are the results of model B. The coefficient of determination was higher for the prediction by model B.

There are several limitations to the present study. First, the heart rate of the anesthetized rats was 300–400 beats/min (5–6.7 Hz), which indicates that the Nyquist frequency may be as low as 2.5 Hz for the heart rate data. The heart rate signal cannot reproduce frequency components above this frequency. Although we included a frequency-independent gain term to explain the flatter portion in the gain plot observed in the experimental transfer function, there is an inherent upper frequency limit to the heart rate control, above which the model is likely to deviate from the experimental transfer function. Second, the frequency-independent gain term suggests the presence of a rapid responding system parallel to the low-pass system in the vagal heart rate control in rats. While the inclusion of the frequency-independent gain term improved the prediction of the dynamic heart rate response to vagal stimulation, the mechanisms for the rapid responding system are largely unknown. Further studies are required to identify the mechanisms and the physiological significance for the rapid responding system observed in rats but not in rabbits.

REFERENCES

[1] T. Kawada, Y. Ikeda, M. Sugimachi, T. Shishido, O. Kawaguchi, T. Yamazaki, et al. "Bidirectional augmentation of heart rate regulation by autonomic nervous system in rabbits," *Am. J. Physiol. Heart Circ. Physiol.*, vol. 271, pp. H288-H295, 1996.

[2] M, Mizuno, T. Kawada, A. Kamiya, T. Miyamoto, S. Shimizu, T. Shishido, et al. "Dynamic characteristics of heart rate control by the autonomic nervous system in rats," *Exp. Physiol.*, vol. 95, pp. 919-925, 2010.

[3] A. A. Shoukas, C. A. Callahan, J. M. Lash, E. B. Haase. "New technique to completely isolate carotid sinus baroreceptor regions in rats," *Am. J. Physiol. Heart Circ. Physiol.*, vol. 260, pp. H300-H303, 1991.

[4] T. Sato, T. Kawada, H. Miyano, T. Shishido, M. Inagaki, R. Yoshimura, et al. "New simple methods for isolating baroreceptor regions of carotid sinus and aortic depressor nerves in rats," *Am. J. Physiol. Heart Circ. Physiol.*, vol. 276, pp. H326-H332, 1999.

[5] T. Kawada, M. Li, A. Kamiya, S. Shimizu, K. Uemura, H. Yamamoto, et al. "Open-loop dynamic and static characteristics of the carotid sinus baroreflex in rats with chronic heart failure after myocardial infarction," *J. Physiol. Sci.*, vol. 60, pp. 283-298, 2010.

[6] P. Z. Marmarelis, V. Z. Marmarelis. Analysis of Physiological Systems. The White-Noise Approach. New York and London: Plenum Press, 1978, pp. 131-178.

Cardiovasc Drugs Ther (2012) 26:217–226
DOI 10.1007/s10557-012-6381-5

H_2 Mediates Cardioprotection Via Involvements of K_{ATP} Channels and Permeability Transition Pores of Mitochondria in Dogs

Akemi Yoshida · Hiroshi Asanuma · Hideyuki Sasaki · Shoji Sanada · Satoru Yamazaki · Yoshihiro Asano · Yoshiro Shinozaki · Hidezo Mori · Akito Shimouchi · Motoaki Sano · Masanori Asakura · Tetsuo Minamino · Seiji Takashima · Masaru Sugimachi · Naoki Mochizuki · Masafumi Kitakaze

Published online: 17 April 2012

Abstract
Purpose Inhalation of hydrogen (H_2) gas has been shown to limit infarct size following ischemia-reperfusion injury in rat hearts. However, H_2 gas-induced cardioprotection has not been tested in large animals and the precise cellular mechanism of protection has not been elucidated. We investigated whether opening of mitochondrial ATP-sensitive K+ channels (mK_{ATP}) and subsequent inhibition of mitochondrial permeability transition pores (mPTP) mediates the infarct size-limiting effect of H_2 gas in canine hearts.
Methods The left anterior descending coronary artery of beagle dogs was occluded for 90 min followed by reperfusion for 6 h. Either 1.3% H_2 or control gas was inhaled from 10 min prior to start of reperfusion until 1 h of reperfusion, in the presence or absence of either 5-hydroxydecanoate (5-HD; a selective mK_{ATP} blocker), or atractyloside (Atr; a mPTP opener).
Results Systemic hemodynamic parameters did not differ among the groups. Nevertheless, H_2 gas inhalation reduced infarct size normalized by risk area (20.6±2.8% vs. control gas 44.0±2.0%; $p<0.001$), and administration of either 5-HD or Atr abolished the infarct size-limiting effect of H_2 gas (42.0±2.2% with 5-HD and 45.1±2.7% with Atr; both $p<0.001$ vs. H_2 group). Neither Atr nor 5-HD affected infarct size per se. Among all groups, NAD content and the number of apoptotic and 8-OHdG positive cells was not significantly different, indicating that the cardioprotection

A. Yoshida · H. Sasaki · S. Yamazaki · M. Asakura · M. Kitakaze (✉)
Department of Cardiovascular Medicine, National Cerebral and Cardiovascular Center, Suita 565-8565, Osaka, Japan
e-mail: kitakaze@zf6.so-net.ne.jp

H. Asanuma
Department of Cardiovascular Science and Technology, Kyoto Prefectural University of Medicine, Suita 565-8565, Osaka, Japan

A. Yoshida · N. Mochizuki
Department of Structural Analysis, National Cerebral and Cardiovascular Research Center, Suita, Japan

S. Sanada · Y. Asano · T. Minamino · S. Takashima
Department of Cardiovascular Medicine, Osaka University Graduate School of Medicine, Suita, Japan

Y. Shinozaki · H. Mori
Department of Physiological Science, Tokai University Graduate School of Medicine, Isehara, Japan

A. Shimouchi
Department of Cardiac Physiology, National Cerebral and Cardiovascular Research Center, Suita, Japan

M. Sano
Department of Cardiology, Keio University School of Medicine, Tokyo, Japan

M. Sugimachi
Department of Cardiovascular Dynamics, Research Institute, National Cerebral and Cardiovascular Center, Suita, Japan

afforded by H_2 was not due to anti-oxidative actions or effects on the NADH dehydrogenase pathway.
Conclusions Inhalation of H_2 gas reduces infarct size in canine hearts via opening of mitochondrial K_{ATP} channels followed by inhibition of mPTP. H_2 gas may provide an effective adjunct strategy in patients with acute myocardial infarction receiving reperfusion therapy.

Key words Hydrogen gas · Reperfusion injury · Myocardial infarction · Mitochondrial K_{ATP} channel · Mitochondrial permeability transition pore

Introduction

Myocardial infarction (MI) is a leading cause of death worldwide, and reduction of infarct size is an important therapeutic goal for patients with acute MI (AMI). The prognosis of AMI has been improved dramatically due to the development of both catheterization techniques and reperfusion therapy by coronary mechanical methods or pharmacological intervention. However, strategies to limit reperfusion injury and thus infarct size have not been well applied in clinical settings [1, 2]. We reported that carperitide limited infarct size in a large scale clinical trial [3]; however, infarct size was reduced by only 14.7%, and the discovery of other therapeutics to limit infarct size may be clinically useful. Interestingly, hydrogen (H_2) has been reported to provide therapeutic benefit for many diseases related to oxidative stress, including cardiovascular disease. There is some evidence that inhalation of H_2 gas limits myocardial infarct size in rats [4, 5]. However, since heart physiology differs significantly in small animals relative to large animals and humans, it cannot be assumed that H_2 would limit infarct size in large animals and humans. Furthermore, the cellular mechanisms underlying H_2-mediated cardioprotection have not been clarified.

Recent accumulated evidence regarding cardioprotection afforded by ischemic pre- or post-conditioning has culminated in the idea that opening of mitochondrial ATP-sensitive K^+ channels (mK_{ATP}) followed by inhibition of mitochondrial permeability transition pores (mPTP) plays a central role in limiting infarct size [6–8]. Indeed, Piot et al. [9] found that administration of the mPTP inhibitor, cyclosporine, at the time of reperfusion limited the size of myocardial infarction in patients with AMI. Ohsawa et al. [10] demonstrated that H_2 has the potential to serve as an antioxidant in preventive and therapeutic applications. Oxygen-derived free radicals are generated inside and outside of cells, and H_2 gas can eliminate hydoxyradical and peroxynitrate because it can penetrate biomembranes and diffuse into the cytosol, mitochondria, and nuclei. If this is the case, H_2 gas may protect mK_{ATP} against ischemic injury, or may directly activate mK_{ATP} followed by the inhibition of mPTP.

Thus, we tested the hypothesis that H_2 gas may reduce reperfusion injury and limit infarct size via the activation of mK_{ATP} and the inhibition of mPTP.

Methods

Animal model and instrumentation

Fifty nine beagle dogs (Oriental Yeast Co., Ltd, Tokyo, Japan) weighing 9 to 10 kg were per-anesthetized with sodium pentobarbital (25 mg/kg iv). All dogs were rapidly intubated and anesthetized with analgesic anesthetics. The control or H_2 gas tank was connected to the respirator 10 min before reperfusion. After baseline hemodynamic assessment, thoracotomy was performed, and the left anterior descending coronary artery (LAD) was ligated just distal to the first diagonal branch. The left carotid artery was catheterized to monitor both aortic blood pressure and heart rate. At the end of each study, animals were euthanized with administration of a high dose of sodium pentobarbital. All procedures were performed in conformity with the Guide for the Care and Use of Laboratory Animals (NIH publication no. 85-23, 1996 revision).

Composition of gas mixture

Gas tanks were obtained from TAIYO NIPPON SANSO Corporation (Osaka, Japan). The control gas tanks were composed of 70% N_2 and 30% O_2. The H_2 gas tanks were composed of 1.3% H_2, 68.7% N_2, and 30% O_2. The H_2 gas concentration was set at 1.3% because higher concentrations create the possibility of explosion. Previous studies showed that 0.5%–4.0% H_2 limited infarct size in rat hearts in vivo, at a flow rate of 1 L/min.

Experimental protocols

After the randomization to either H_2 gas (n=18) or control gas (n=18), the LAD of the beagle was occluded for 90 min followed by reperfusion for 6 h. Either H_2 gas or control gas was inhaled (3.36 L/min) 10 min prior to reperfusion until 1 h of reperfusion. In addition, we intravenously administered either 5-hydroxydecanoate (5-HD, Sigma; 10 mg/kg i.v.), or atractyloside (Atr, Sigma; 2.5 mg/kg i.v.), for 5 min before gas inhalation [H_2 gas with 5-HD (n=6) or Atr (n=6) and control gas with 5-HD (n=6) or Atr (n=6)]. In all groups, infarct size was assessed after 6 h of reperfusion. We also investigated apoptosis in the myocardium adjacent to the infarct area using TUNEL staining. In addition, we counted the incidence of lethal arrhythmia, defined as more than 15 consecutive premature ventricular contractions (VPC) or ventricular fibrillation (Vf) from 10 min before reperfusion to 60 min after the onset of reperfusion.

Measurement of infarct size and myocardial collateral blood flow

We measured both area at risk and infarct area 6 h after the onset of reperfusion as described previously [11]. These parameters were evaluated by Evans blue and triphenyltetrazolium chloride (TTC) staining, respectively. Infarct size was calculated as [infarct area/area at risk] × 100(%).

Regional myocardial blood flow was determined by the microsphere technique. Non-radioactive microspheres (Sekisui Plastic Co., Ltd., Tokyo, Japan) are made of inert plastic labeled with niobium (Nb) and bromine (Br) as described in detail in previous study [12]. Microspheres were suspended in isotonic saline with 0.01% Tween80 to prevent aggregation. The microspheres were ultrasonicated for 5 min followed by 5 min of vortexing immediately before injection. Approximately 1 mL of the microsphere suspension ($2–4\times10^5$ spheres) was injected into the left atrium at 80 min after the start of coronary occlusion.

The X-ray fluorescence of stable heavy elements was measured by a wavelength dispersive spectrometer (PW 1480, PHILLIPS Co., Ltd.). The specifications of this X-ray fluorescence spectrometer have been described previously [12]. In brief, when the microspheres are irradiated by the primary X-ray beam, the electrons fall back to a lower orbit and emit measurable energy. The energy level of the X-ray fluorescence depends on the characteristics of each element. Therefore, it was possible to quantify the X-ray fluorescence of several differently labeled microspheres in the mixture. Regional myocardial collateral blood flow was calculated according to the following formula: time flow = (tissue count) × (reference flow)/(reference count), and was expressed in mL/g wet weight/min.

Terminal Deoxynucleotidyl transferase-mediated dUTP nick-end labeling (TUNEL)

The myocardial tissue samples were taken from the border zone of dogs in the control, H_2, control+5-HD, H_2+5-HD, control+Atr and H_2+Atr groups (n=3 each). The border zone was chosen as the region within 4 mm from the infarct zone. These were fixed in 10% buffered formalin, embedded in paraffin, and serially sectioned in the frontal plane at 5-μm thickness. To assess myocardial apoptosis, analysis by TUNEL method was performed according to the protocol supplied with the in situ apoptosis detection kit, the Apop Tag Peroxidase In Situ Apoptosis Detection Kit (S7100, MILLIPORE). The sections were then shortly counterstained with hematoxylin and eosin to visualize the cells. TUNEL-positive cell nuclei and total cell nuclei stained metylgreen were counted in 7–10 random high-power fields (×200). The amount of TUNEL-positive cells was expressed as a percentage of the total amount of cells (n=1,500).

Immunohistochemistry for either 8-OHdG or NAD+ of the Reperfused myocardium

The myocardial tissue samples were taken from the border zone between ischemic and non-ischemic areas in the control, H_2, H_2+5-HD, H_2+Atr, control+5-HD and control+Atr groups (n=3 each). After 90 min of ischemia followed by 6 h of reperfusion, hearts were excised and the myocardial tissue samples were taken from the border zone. The border zone was chosen as the region within 4 mm from the infarct zone. These were fixed in 10% buffered formalin, embedded in paraffin, and serially sectioned in the frontal plane at 5-μm thickness. The paraffin sections were deparaffinized in xylene, rehydrated using various grades of ethanol, and pretreated with 10 mM citric acid for 40 min at 95°C. For immunostaining, sections stained with anti-8OH-dG (MOG-020P; Japan Institute for the Control of Aging; 1:100) antibodies overnight at 4°C. Secondary antibodies conjugated Simple Stain Rat (MAX-PO MULTI 414191, NICHIREI Bioscience inc. Japan; undiluted) were applied for 30 min at room temperature. The sections were then shortly counterstained with hematoxylin and eosin to visualize the cells. Four slides were randomly examined using a defined rectangular field area with magnification (×40). The data were represented as the number of 8OH-dG positive cells per field.

Since mPTP may be opened via oygen-drived free radicals via the NADPH oxidase, we also investigated the myocardial NAD+ contents as well. We used 18 dogs for NAD assessment in the control, H_2, H_2+5-HD, H_2+Atr, control+5-HD and control+Atr groups (n=3 each). The myocardial tissue in the border zone was quickly placed into liquid nitrogen and stored at −80°C. For the measurement of NAD+, 40 mg of border zone tissue was homogenized. An equal amount of protein from the homogenized tissue of each group was used for the NAD+/NADH Colorimetric assay kit (Cat# CY-1253; Cyclex Co., Ltd).

Exclusion criteria

To ensure that all animals used in the present study were healthy and had been exposed to a similar extent of ischemia, the following standards were employed for the exclusion of unsatisfactory dogs: (1) subendocardial collateral blood flow greater than 15 mL/100 g/min; (2) heart rate greater than 170 beats/min; and (3) more than two consecutive attempts required to terminate ventricular fibrillation (Vf) using low-energy DC pulses applied directly to the heart.

Statistical analysis

Statistical analysis was performed using two-way repeated measures analysis of variance (ANOVA) when data were

compared over the time course of the change between groups. Analysis of covariance between regional collateral flow in the inner half of the left ventricular wall and infarct size was described previously [11]. Other data were compared using one-way fractional analysis of variance. If statistical significance was found for a group, time effect, or group-by-time interaction, further comparisons were made with paired t tests between all possible pairs of the five groups at individual time points. Results were expressed as means ± SEM, with $p<0.05$ considered statistically significant.

Results

Among the 59 dogs, 23 were excluded due to Vf or excessive myocardial collateral blood flow (>15 mL/100 g/min). The remaining 36 dogs completed the protocols satisfactorily and were included in the data analysis. None of the pharmacological interventions such as H_2 gas, control gas, 5-HD, or Atr, altered systemic blood pressure or heart rate during the experimental protocols (Table 1).

Inhalation of H_2 gas just prior to reperfusion following 90 min of ischemia reduced infarct size normalized by risk area (20.6±2.8% vs. 44.0±2.0%; $p<0.001$) (Fig. 1). Intriguingly, the administration of either 5-HD or atractyloside (Atr) blunted the H_2 gas induced limiting effect on infarct size (42.0 ±2.2% in 5-HD vs. 45.1±2.7% in Atr; $p<0.001$ and $p<0.001$ vs. H_2 gas group). Neither 5-HD nor atractyloside per se affected infarct size. There were no differences in either risk area or collateral flow during the ischemic period among the groups (Fig. 2). Figure 3 shows the regression plots of the area at risk vs. collateral flow. Inhalation of H_2 gas mediated the substantial cardioprotection irrespective of collateral flow, which was again blunted by either 5-HD or atractyloside.

On the other hand, we observed apoptosis using TUNEL staining in the myocardium in each group; there were no differences in the extent of apoptosis in the groups (36.0± 1.8, 26.5±6.9, 33.0±1.4, 35.6±1.5, 35.0±1.3 and 35.7±1.4% in the control group, the H_2 gas group, the H_2 gas with 5HD group, the H_2 gas with Atr group, the control gas with 5HD group, and the control gas with Atr group, respectively).

We observed the incidence of lethal arrhythmia throughout the experiments in all groups from 10 min before reperfusion to 60 min after the onset of reperfusion (Table 2). The presence of either Vf or VPC longer than 15 consecutive beats was defined as lethal arrhythmia in this study. The incidence of lethal arrhythmia in the reperfusion period tended to decrease by H_2 gas although there were no significant differences. This tendency was blunted by either 5-HD or Atr. These data indicate that H_2 gas may affect the incidence of fatal ventricular arrhythmias during the reperfusion period, but it is unknown whether this effect is attributable to a potential primary anti-arrhythmic effect of H_2 gas or merely secondary to the infarct size-limiting effects of H_2 gas.

The number of 8-OHdG (a biomarker of oxidative stress) positive cells, tended to decrease in H_2 group relative to the other groups, however there was no significant difference (Fig. 4). We also observed no relation between the number

Table 1 Effect of H_2 gas on systemic hemodynamic parameters

Groups	Baseline	Isc-60	Isc-90	Rep-60	Rep-120	Rep-180	Rep-240	Rep-300	Rep-240
Mean blood pressure (mmHg)									
Control gas	101±2	103±2	104±2	98±2	102±2	101±3	103±3	99±3	100±2
H_2 gas	105±4	97±2	98±3	96±3	100±2	101±3	99±2	101±2	103±1
H_2 gas + 5HD	105±2	105±2	106±1	95±3	98±3	101±3	103±1	102±0	100±4
H_2 gas + Atr	98±3	98±3	102±3	98±1	100±1	101±1	102±1	102±2	103±1
Control gas + 5HD	104±2	101±2	101±1	102±2	103±2	101±3	103±2	98±3	100±4
Control gas + Atr	102±1	102±4	100±2	96±1	103±2	100±3	103±2	104±2	102±1
Heart rate (beats/min)									
Control gas	136±3	138±2	137±2	132±2	131±1	135±3	135±4	133±4	133±4
H_2 gas	139±3	138±3	140±4	133±3	134±4	134±5	134±4	134±5	132±4
H_2 gas + 5HD	135±3	130±3	129±4	129±3	129±4	130±3	129±4	129±4	130±3
H_2 gas + Atr	134±2	135±4	130±4	129±3	129±2	129±3	129±2	128±3	129±3
Control gas + 5HD	134±4	135±3	135±3	135±2	129±3	131±5	132±5	130±5	129±5
Control gas + Atr	137±2	137±2	135±3	136±2	137±3	135±4	135±2	135±3	136±2

Values are expressed as mean ± SEM. Isc-60 and Isc-90 show 60 and 90 min after the onset of myocardial ischemia, respectively. Rep-60, Rep-120, Rep-180, Rep-240, Rep-300 and Rep-360 show 60, 120, 180, 240, 300 and 360 min after the onset of reperfusion, respectively. There were no significant changes of theses parameters among the six groups

5HD = 5-hydroxydecanoate; Atr = Atractyloside